Estimation of Maximum Compressive Load for Circular Tubes under Axial Impact

D.H. Chen[1] and K. Ushijima[2]

1Department of Mechanical Engineering, Faculty of Engineering, Tokyo University of Science, Tokyo, 1628601, Japan

2Department of Mechanical Engineering, Faculty of Engineering, Kyushu Sangyo University, Fukuoka, 8138503,Japan

Abstract   *The influence of impact velocity on the crushing behaviour of cylindrical shells subjected to an axial impact was investigated using a finite element analysis. The effects of the material properties, tube geometries and impact velocity V_0 on the initial peak stressσ_1 are explored.*

In this study, the applied material is assumed to be insensitive to the strain rate, and the effect of impact velocity is discussed as an inertia effect. It is shown that the initial peak stressσ_1 during dynamic loading increases with increase of the impact velocity V_0, which is due to the fact that the displacement in radial direction is delayed as the velocity V_0 increases. Also, based on our numerical simulations, the peak stressσ_1 can be regarded as a function of the ratio of tube thickness to radius t/R, hardening modulus to Young's modulus E_h/E and impact velocity to elastic stress wave speed V_0/c. Moreover, an approximate equation to evaluate the peak stress is proposed and in good agreement with the FEM results and other researcher's results under a relatively low impact velocity ($V_0 < 40m/s$).

Keywords   Elastic-plastic cylindrical shells, Axial impact, Energy absorption, FEM

1.Introduction

Thin-walled structures such as circular and square tubes have been widely used in automotive and aerospace engineering as impact energy absorbing devices. A large number of studies concerning the static and dynamic response of thin-walled tubes subjected to axial load have been conducted by many researchers, and investigated some important parameters such as crushing distance, the peak load and the buckling shape in crashworthiness design [1-13]. Figure 1 shows a schematic of compressive axial stressσ_x and displacement U_x for a cylindrical tube subjected to axial loading.

The purpose of this study is to explore the effect of impact velocity on the peak load for circular tubes, and to propose an empirical equation to estimate the peak load by numerical simulation.

2.Method of Analysis

In this study, the dynamic numerical simulation of the impact crush test was carried out using the non-linear FE commercial code, MSC.Dytran. The geometry of the FE model and its boundary condition is shown in Fig.2. The model is struck from the upper edge by a rigid mass M having an initial kinetic energy $T_0 = MV_0^2/2 = 99$ kJ. In the FE model, 4-node Key-Hoff shell elements(QUAD4, PSHELL) with three integration points are used to evaluate domain integrals, and the whole model is divided into 1440 elements. Here, parameters L, t and R are the tube length, thickness and mean radius, respectively. Also, the lower end of a tube is fixed to another rigid body, and a contact condition between the tube and the striker, and a self-contact condition at the inner and the outer surface of the tube are defined with the dynamic and static frictional coefficients of 0.2 and 0.3, respectively.
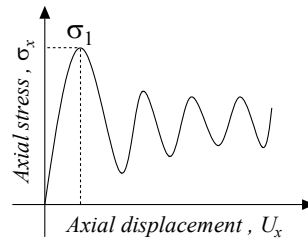
Fig.1. Schematic of axial compressive stress-displacement relationship for a tube subjected to axial impact
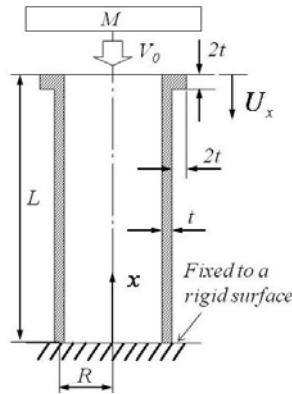
Fig.2. Shell geometry and loading condition

The analyzed FE model with a density ρ=2685 kg/m^3 is assumed to be isotropic, and to obey the Mises yield criterion with strain hardening, and a strain rate insensitive bilinear relationship between the uniaxial stress and strain as:

$$\sigma = \begin{cases} E\varepsilon & \left(\varepsilon \le \sigma_y / E\right) \\ \sigma_y + E_h\left(\varepsilon - \sigma_y / E\right) & \left(\varepsilon > \sigma_y / E\right) \end{cases} \quad (1)$$

Here, the Young's modulus, E, yielding stress, σ_y and hardening coefficient, E_h are assumed to be 72.4 GPa, 72.4 MPa and 3.62 GPa, respectively.

All models in our calculation have the same tube length L=150 mm, mean radius R=25 mm and thickness t=1 mm, unless otherwise mentioned.

3.Results and Discussion

3.1 Effect of Impact Velocity V_0 on the initial peak stress σ_1
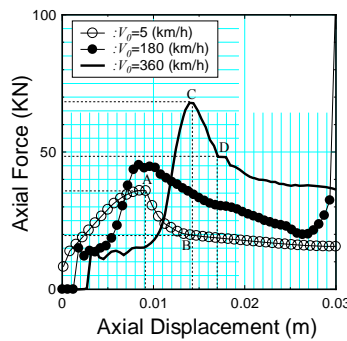
Fig.3. Comparison of axial force and displacement behaviour for a tube under different impact velocity V_0

Figure 3 shows comparisons of axial compressive force and displacement diagram for a tube under the impact velocity V_0=5, 180 and 360 km/h.

Also, the deformed shapes at the initiation of the initial peak stress and soon after the stress for the case of V_0=5 km/h and 360 km/h are shown in Fig.4. It is evident from Fig.4 that the initial peak stress is associated with the initiation of local buckling deformation which occurs near the upper and lower ends of a tube. From the relationship between the axial load and displacement for each V_0 which is shown in Fig.3, the initial peak stress can be calculated and summarized in Fig.5. Also in Fig.5, quasi-static buckling stress for the tube obtained by implicit finite element code, MSC.Marc, is shown by a dashed line. It is found from this figure that the initial peak stressσ_1 for a lower impact velocity is almost equal to the value of the quasi-static result, and the stress value becomes higher as the impact velocity V_0 increases.

<div align="center">(a)   (b)   (c)   (d)</div>
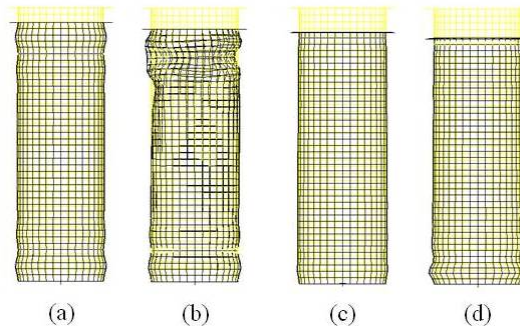
Fig.4. Comparisons of deformed shape at points 'A', 'B', 'C' and 'D' in Fig.3. 'A': buckling point for V_0=5(km/h); 'B': point just after buckling for V_0=5(km/h); 'C': buckling point for V_0=360(km/h); 'D': point just after buckling for V_0=360 (km/h)
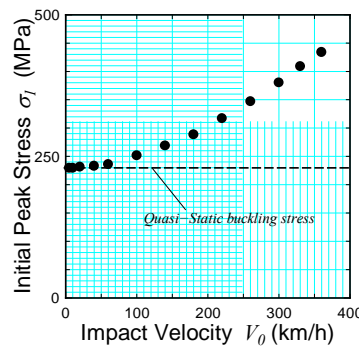
Fig.5. Variation of peak stress σ_1 with impact velocity V_0
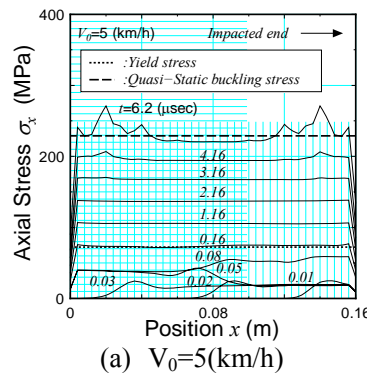
<div align="center">(a) V_0=5(km/h)</div>

Figure 6 illustrates propagations of the stress wave in the axial direction for V_0=5 km/h (Fig.6(a)) and 360 km/h (Fig.6(b)) until the initial peak stress occurs. Also in Figure 6, values of the yield stressσ_y and the quasi-static buckling stress are shown by dotted and dashed lines, respectively. It is evident from Fig.6(a) that for the case of a lower impact velocity(V_0=5 km/h),

the amplitude of the stress wave in axial direction at the initiation of impact is relatively small, and the stress wave travels and reflects many times along the tube until the local buckling deformation arises near the fixed end. In the end, the axial stress distribution developing over the tube becomes almost uniformly at t=0.16μs, and its amplitude increases stably to the quasi-static buckling stress. On the other hand, for the case of a higher impact velocity (Fig.6(b)), the development of axial stress distribution apparently differs from that for a lower impact velocity(Fig.6(a)).

(b) V_0=360(km/h)
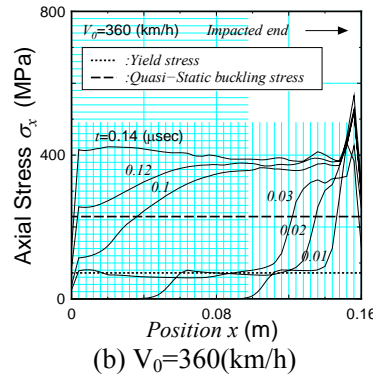
Fig.6. Axial stress distribution until the initiation of the peak stressσ_1

In Fig.6(b), the stress concentration can be found at x=0.156 m. Such a stress concentration occurs by the existence of the flange at the impacted end, and does not affect the overall buckling behaviour of a circular tube. It is evident from Fig.6(b) that the amplitude of the stress wave bigger than the value of quasi-static buckling stress develops near the impacted end at the beginning. However, such the high stress field is relatively narrow, and no buckling behaviours seem to be observed even if the amplitude of stress wave is bigger than that of the quasi-static result. Moreover, even though the axial stress developing over the tube becomes larger than the quasi-static result at t=0.12μs, no buckling can be observed. Finally, the local buckling can be observed at t=0.14μs when the amplitude of the axial stress is almost twice larger than the quasi-static buckling stress. The mechanism of the buckling for circular tubes under higher impact velocities will be discussed as follows.
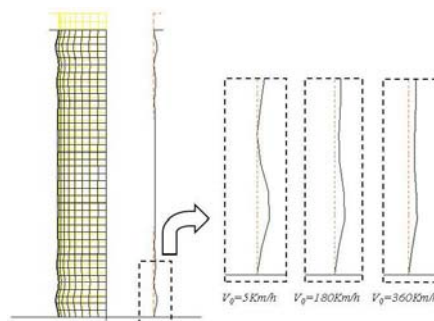
Fig.7. Comparisons of deformed shape near the fixed end at the initiation of the peak stressσ_1

Based on the previous work concerning the quasi-static axial compressive behaviour for circular tube, it is evident that the initial peak stress is associated with the sufficient local bending deformation which is observed near the tube end. That is, during the axial compression, the tube seems to expand in radial direction, but near the tube end, such a movement is restricted by the existence of the fixed boundary condition. As a result, the local bending deformation can be observed near the tube end, and the local bending deformation is necessary for initiating the buckling behaviour. Figure 7 shows comparisons of deformed shape near the fixed end when the initial peak stress is observed for some cases of impact velocity V_0=5 km/h, 180 km/h and 360

km/h. It is evident that for the case of a higher impact velocity, the amount of the local bending deformation is smaller than that under a slower impact velocity. In order to initiate the buckling behaviour where the smaller amount of the local bending deformation occurs under higher impact velocity, that is, in order to increase the radial displacement, a large amount of axial stress should be needed. Therefore, it could be understood that the reason why the initial peak stress increases as increase of the impact velocity V_0 is due to the fact that the impact for a higher impact velocity causes a smaller radial displacement than that for a lower impact velocity. Moreover, the reason why the bending deformation decreases as V_0 increases can be explained by the radial inertia effect. That is, the more faster the impact velocity becomes, the more rapidly the axial stress increases, but the expansion in radial direction would be delayed by the radial inertia effect. Such a mechanism can be observed in Fig.8.
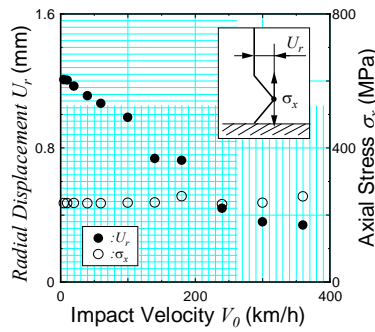
Fig.8.Variation of radial displacement U_r and axial stress σ_x at the apex of wrinkle with impact velocity V_0
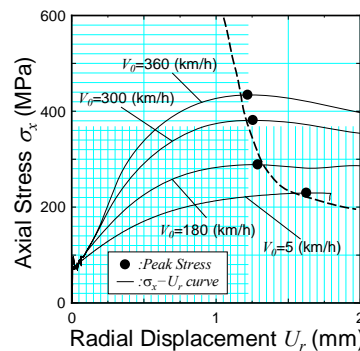
Fig.9. Variation of axial stressσ_x with radial displacement U_r at the apex of wrinkle for V_0=5, 180, 300 and 360 (km/h)

Figure 8 presents the relationship between the radial displacement U_r and the impact velocity V_0 under almost the same amount of the axial stressσ_x. It is evident that the displacement U_r decreases as increase of V_0 even if the same amount ofσ_x occurs. Moreover, the relationship between the axial stressσ_x and the radial displacement U_r for four cases of V_0= 5, 180, 300 and 360 km/h are chased and the initial peak stress for every V_0 is summarized in Fig.9 by marks ●. From the figure, the reason why the higher velocity causes the larger initial peak stress can be explained as follows. While the axial stress increases by propagating the stress waves over the tube, the radial displacement U_r develops by the axial compression, but the rate of U_r relatively decreases as increase of V_0. As a result, the axial stress increases by the stress wave reflecting many times until the sufficient radial displacement can be reached for initiating the local buckling.

    In order to discuss the influence of V_0 on the peak stress quantitatively, an effective parameter considering the effect of mechanical properties on the inertia effect is needed. Figure 10 shows the relationship between the normalized axial stress σ_x/E and displacement U_x/L for

three cases of a tube problem having different elastic modulus E, tube density ρ and the impact velocity V_0. In the figure, parameter c represents the elastic wave speed for a one-dimensional rod, and can be shown as $(E/\rho)^{1/2}$. Here, all models have different values of E, ρ and V_0, but keep the same ratio V_0/c. It is evident that all models behave the same response of the axial stress σ_x/E and U_x/L diagram. Strictly speaking, the elastic and the plastic wave speed for a circular tube are distinct from the elastic wave speed c for a one-dimensional rod. However, based on the fact that the relationship between the normalized axial stress σ_x/E and displacement U_x/L is the same under the same V_0/c, the non-dimensional parameter V_0/c can be used for evaluating the effect of impact velocity on the initial peak stress σ_1.
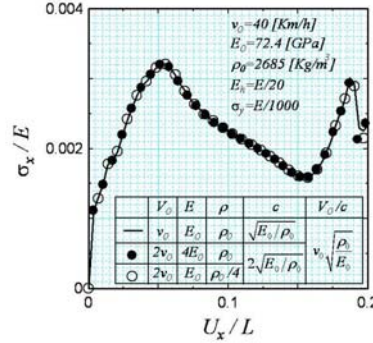
Fig.10. Normalized axial compressive stress and displacement behaviour for tubes having the same ratio of V_0/c

3.2 Effects of tube geometries and material properties on the initial peak stress

As the other effective parameters for the dynamic initial peak stress σ_1, tube geometries (such as mean radius, R and thickness, t) and material properties (such as Young's modulus, E, hardening coefficient, E_h and yield stress, σ_y) can be given, and the effects of these parameters on σ_1 are discussed as follows.
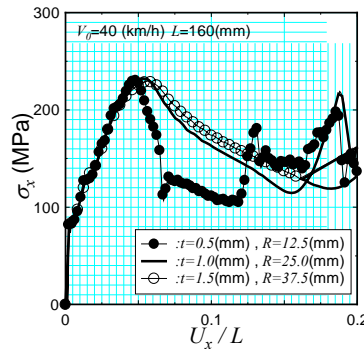
Fig.11. Comparison of the compressive stress and displacement behaviour for tubes having the same ratio of tube thickness to radius t/R

Figure 11 summarizes effects of mean radius R and thickness t on the axial stress and displacement behaviour for tubes having different tube radius R and thickness t, but the same ratio of t/R. It is evident from Fig.11 that if the ratio of t/R has the same value, the initial peak stress σ_1 has the same value.
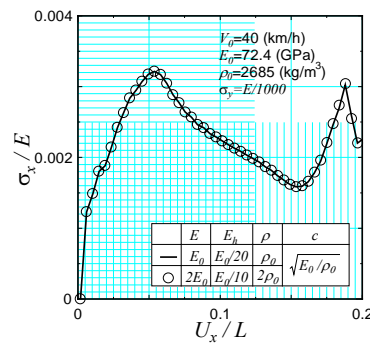
Fig.12. Normalized axial compressive stress σ_x/E and displacement U_x/L behaviour for tubes having the same ratios of E_h/E and V_0/c

Figure 12 shows the comparison of the relationship between two tubes having the different E and E_h but the same ratio of E_h/E. In the figure, the stress value is normalized by E. It can be observed from Fig.12 that the normalized initial peak stress σ_1/E can be arranged as a function of the ratio, E_h/E.

Moreover, the yield stress σ_y for a tube also affects the initial peak stress, but if the value σ_y is quite smaller than the peak stress σ_1, the effect seems to be negligible.

From the above results and discussions, the normalized initial peak stress σ_1/E for a tube obeying a bilinear stress and strain relationship can be expressed by a function composed of four parameters, V_0/c, t/R, E_h/E and σ_y/E as:

$$\frac{\sigma_1}{E} = f_1\left(\frac{V_0}{c}, \frac{t}{R}, \frac{E_h}{E}, \frac{\sigma_y}{E}\right) \tag{2}$$

Figure 13 shows the relationship between the normalized impact velocity V_0/c and the peak stress σ_1/E for some combinations of ratios, t/R, E_h/E and σ_1/E. It is clear from the figure that the stress σ_1/E increases linearly with the parameter $(V_0/c)^2$. Also, the slope and intersect of the relationship depend on these ratios, E_h/E and t/R.
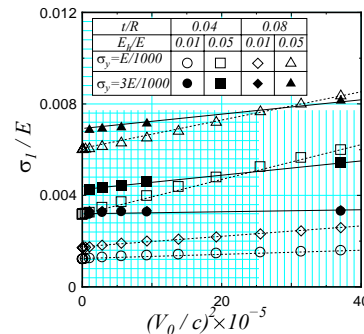
Fig.13. Normalized impact velocity V_0/c and the peak stress σ_1/E for some combinations of t/R, E_h/E and σ_y/E

Based on these charateristics, the normalized initial peak stress σ_1/E can be written by the following type of equation as:

$$\frac{\sigma_1}{E} = C_1\left(\frac{V_0}{c}\right)^2 + C_2 \tag{3}$$

where,

$$C_1 = f_2\left(,\frac{t}{R},\frac{E_h}{E},\frac{\sigma_y}{E}\right), C_2 = f_3\left(,\frac{t}{R},\frac{E_h}{E},\frac{\sigma_y}{E}\right).$$

Equation (3) means that the initial stress can be expressed by the sum of the inertial term including the parameter V_0/c and the quasi-static term for $V_0=0$.

Here, the quasi-static term C_2 has already been discussed in the previous study[11], and proposed an approximate equation as follows:

$$C_2 = \left.\frac{\sigma_1}{E}\right|_{static}$$

$$= \begin{cases} \dfrac{t}{\sqrt{3(1-v^2)}R} & (t/R \le x_0) \\[3mm] \dfrac{\sigma_y}{E} + \dfrac{t}{2R}\cdot\left(\dfrac{E_h}{E}\right)^{0.7(1-E_h/E)}\left(1-e^k\right) & (t/R > x_0) \end{cases} \qquad (4)$$

where,

$$x_0 = \frac{\sigma_y\sqrt{3(1-v^2)}}{E}, k = \frac{-22\,E_h/E}{\sqrt{\sigma_y/E}}\left(\frac{t}{R} - x_0\right)$$

Figure 14 shows comparisons of the parameter C_2 obtained by FEM and its approximation obtained by Eq.(4). In the figure, results for $\sigma_y/E=1/1000$ and $3/1000$ correspond to solid and dotted lines, respectively. It is clear that both results coincide with each other, and the approximate equation which is shown as Eq.(4) can be used to estimate the quasi-static peak stress with a good accuracy.
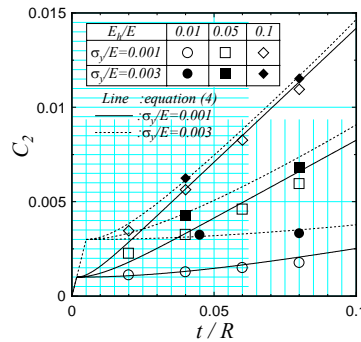
Fig.14. Comparisons of quasi-static term C_2 in Eq.(3) for tubes having some combinations of $t/R, \sigma_y/E$ and E_h/E

In Figure 15, results of the parameter C_1 for some ratios, $E_h/E, \sigma_y/E$ and t/R are summarized. It is found from the figure that the parameter C_1 increases with increase of E_h/E, and its value becomes larger as the ratio of tube thickness to radius t/R decreases. Also, the value C_1 depends on the yield stress σ_y. For example, C_1 for $t/R=0.02$ and 0.08 under the same ratios, $E_h/E=0.1$ and $\sigma_y/E=0.001$ are almost equal to 13.0 and 8.0, respectively, so that the difference between them is almost 5.0. However, by concerning the term $(V_0/c)^2$, for example, if the impact velocity V_0 is 100km/h, the order of the parameter $(V_0/c)^2$ is about 10^{-5}, and the scale of the difference is one digit smaller than the parameter C_2. Based on the fact, the parameter C_1 can be written by the following equation as:

$$C_1 = 50\left(\frac{E_h}{E}\right)^{0.7} \qquad (5)$$

and shown in Fig.15 as a solid line.
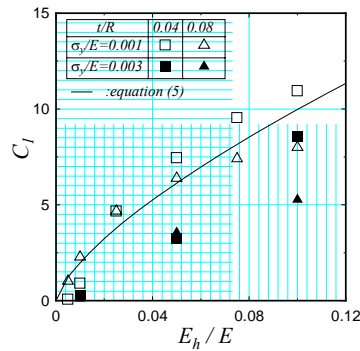
Fig.15. Comparisons of quasi-static term C_1 in Eq.(3) for tubes having some combinations of $t/R, \sigma_y/E$ and E_h/E

Consequently, an approximate equation for the non-dimensional initial peak stress for a cylindrical tube subjected to axial impact load is proposed in this paper as follows:

$$\frac{\sigma_1}{E} = 50 \left(\frac{E_h}{E} \right)^{0.7} \left(\frac{V_0}{c} \right)^2 + \left. \frac{\sigma_1}{E} \right|_{static} \tag{6}$$
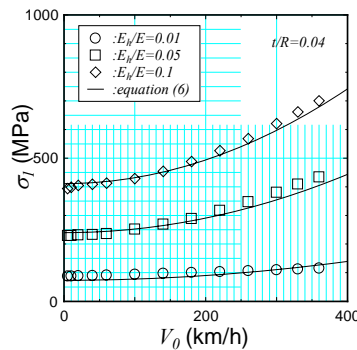
(a) for the case of t/R=0.04
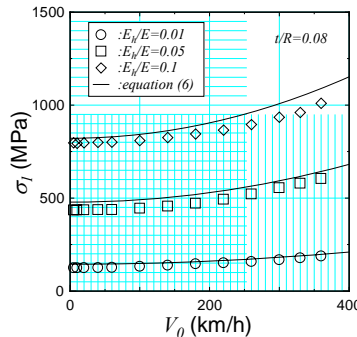
(b) for the case of t/R=0.08

Fig.16. Estimation of the peak stress σ_1 under some cases of impact velocity V_0

Figure 16 shows the relationship between the initial peak stress and the impact velocity for some cases of E_h/E for the ratio of t/R=0.04 (Fig.16(a)) and 0.08 (Fig.16(b)). In these figures, solid lines correspond to the approximate results obtained by Eq.(6), and the symbols show the numerical results obtained by FEM. It is clear from these figures that the predicted σ_1/E agrees well with the numerical results for a wide range of impact velocity V_0.

4. Validation of the proposed prediction for σ_1

In order to check the validity of the proposed prediction for σ_1 as shown in Eq.(6), the same impact problem studied by Karagiozova and Jones[5] is examined and compared the prediction with their results in Fig. 17. In the figure, the solid line shows the approximation by Eq.(6), and dotted line and solid circles are the predictions and FEM results which can be found in Karagiozova and Jones' paper[5]. Here, the model is intended for a circular tube made of aluminium alloy, and the material and geometrical parameters of the model are shown in Fig. 17. It is evident that for relatively low impact velocity ($V_0<40$m/s), the proposed approximation gives a good agreement with numerical results obtained by Karagiozova and Jones[5], which means that the proposed approximation can be effectively used for estimating the initial peak stress σ_1 under a relatively low impact velocity.
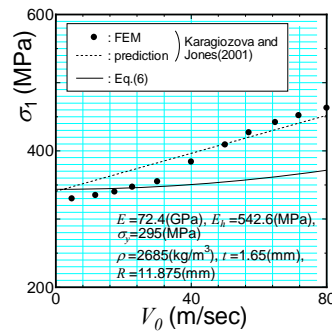
Fig.17. Comparison of estimating the peak stress σ_1 under some cases of impact velocity V_0

5. Conclusion

In this paper, large displacement numerical simulation based on FEM is undertaken to explore the relationship between the impact velocity V_0 and the initial peak stress σ_1 for circular tubes when subjected to an axial impact.

Based on our numerical results, the following points have been revealed.

(1) The initial peak stress σ_1 becomes higher with increases of the impact velocity V_0. That is because the local displacement U_r in radial direction decreases as V_0 increases, under the same axial stress σ_x.

(2) The initial peak stress σ_1 can be expressed by the sum of a term including V_0/c and a term obtained by quasi-static numerical simulation.

(3) The proposed approximate equation for σ_1 can be effectively used under low impact velocity ($V_0<40$m/s).

References

[1] Karagiozova D. and Alves M., Jones N., Inertia effects in axisymmetrically deformed cylindrical shells under axial impact. Int. J. Impact Engng. 24(10)(2000) 1083-1115.

[2] Karagiozova D. and Alves M., Transition from progressive buckling to global bending of circular shells under axial impact – Part I: Experimental and numerical observations. Int. J. Solids Struct. 41(5-6)(2004) 1565-1580.

[3] Karagiozova D. and Alves M., Transition from progressive buckling to global bending of circular shells under axial impact – Part II: Theoretical analysis. Int. J. Solids Struct. 41(5-6)(2004) 1581-1604.

[4] Karagiozova D. and Jones N., Dynamic effects on buckling and energy absorption of cylindrical shells under axial impact. Thin-Walled Struct. 39(7)(2001) 583-610.

[5] Karagiozova D. and Jones, N., Influence of stress waves on the dynamic progressive and dynamic plastic buckling of cylindrical shells. Int. J. Solids Struct. 38(38-39)(2001) 6723-6749.

[6] Karagiozova D. and Jones, N., On dynamic buckling phenomena in axially loaded elastic-plastic cylindrical shells. Int. J. of Non-Linear Mech. 37(7)(2002) 1223-1238.

[7] Karagiozova D. and Jones, N., On the mechanics of the global bending collapse of circular tubes under dynamic axial load - Dynamic buckling transition. Int. J. Impact Engng. 35(5)(2008) 397-424.

[8] Karagiozova D., Nurick G.N. and Yuen S.C.K., Energy absorption of aluminium alloy circular and square tubes under an axial explosive load. Thin-Walled Struct. 43(6)(2005) 956-982.

[9] Lu G. and Mao R., A study of the plastic buckling of axially compressed cylindrical shells with a thick-shell theory. Int. J. Mech. Sci. 43(10)(2001) 2319-2330.

[10] Rusinek A., Zaera R., Forquin P., and Klepazko, J.R., Effect of plastic deformation and boundary conditions combined with elastic wave propagation on the collapse site of a crash box. Thin-Walled Struct. 46(10)(2008) 1143-1163.

[11] Ushijima K., Haruyama S. and Chen D-H. Evaluation of first peak stress in axial collapse of circular cylindrical shell. Trans. JSME. Series A 70(700)(2004) 1695-1702.

[12] Wei Z.G., Yu J.L. and Batra R.C. Dynamic buckling of thin cylindrical shells under axial impact. Int. J. Impact Engng. 32(1-4)(2005) 575-592.

Zhao H. and Abdennadher S. On the strength enhancement under impact loading of square tubes made from rate insensitive metals. Int. J. Solids Struct. 41(24-25)(2004) 6677-669.